Phonons, charge and spin in correlated systems

Macridin, Alexandru; Sawatzky, G.A

Chapter 6

Multi-Band Hubbard Model

6.1 Introduction

The high T_c cuprate superconductors are layered materials with relatively complex structures and chemical composition. They are highly correlated, with an effective bandwidth roughly equal to the effective local Coulomb interaction. The short-range correlations are known to play a paramount role in these materials. Therefore the DCA technique we introduced in Chap. 5 we believe to be an ideal tool for the investigation of these systems. The undoped materials are antiferromagnetic insulators with a gap of approximatively 2 eV. Upon doping the antiferromagnetism is destroyed and the system becomes superconducting. At small doping, in the proximity of the antiferromagnetic phase, the normal state physics cannot be described in terms of Fermi liquid theory and is characterized by the presence of a pseudogap. An essential demand of every successful theory is to capture all these fundamental features at the same time.

A common characteristic all the cuprate materials share is the presence of quasi-two-dimensional CuO_2 planes. It is widely believed that the relevant low-energy physics is described by the degrees of freedom belonging to these planes. The full complexity of the orbital chemistry of just the CuO_2 planes and the strong Coulomb repulsion on the Cu ions would lead to models which are very difficult to study with conventional techniques.

Starting from the insulating parent materials, the photoemission experiments show that the first electron-removal states have primarily oxygen p character, unlike the first electron-addition states which have Cu d character. This fact places these materials in the charge-transfer region of Zaanen-Sawatzky-Allen scheme [1]. Early on, considering the ligand field symmetry and band structure calculation [2–4], it was realized that the most important degrees of freedom are the Cu $d_{x^2-y^2}$ and the in-plane O p_σ orbitals. Therefore, one of the first models proposed to describe the physics of high T_c materials was the so called *three-band Hubbard model* introduced by Varma *et al.* [5] and Emery *et al.* [6, 7]. This Hamiltonian considers only the oxygen p_σ and the correlated cooper $d_{x^2-y^2}$ orbitals.

One step further was taken by Zhang and Rice [8] who argued that the low-energy physics of the hole-doped superconductors can be described by a one-band t-J model or by the closely related single-band Hubbard model. Starting from the *three-band model* and neglecting the oxygen dispersion, Zhang and Rice showed , within second order perturbation theory, that an extra hole added into the oxygen band binds strongly with a

hole on the Cu, forming an on-site singlet. This singlet state, which has zero spin can be thought as moving through the lattice like a hole in an antiferromagnetic background. Consequently, the physics can be described by a one-band t-J model and equivalently the low-energy electron-removal states can be mapped onto a lower Hubbard band of a single-band Hubbard model.

Pertinent criticism to these simplified models were raised by various authors. With respect to the Cu degrees of freedom, H. Eskes *et al.* [9] stressed the possible importance of the other d orbitals. In order to determine the relevance of different parameters and orbitals, they calculated the CuO_4 cluster's states considering all 12 O p and all 5 Cu d orbitals and compared the results with the photoemission and with the x-ray absorption experimental spectra. The $d_{3z^2-r^2}$, d_{xy}, d_{xz} and d_{yz} orbitals enter in the formation of states separated only by $\approx 1.5\ eV$ from the Zhang-Rice singlet states, this separation being much smaller than the Zhang-Rice singlet-triplet splitting ($\approx 3.5\ eV$). Especially the $d_{3z^2-r^2}$ orbitals seem to be important since they are strongly stabilized by the presence of short bond lengths with the apex oxygen atoms. Therefore, our model which will neglect all the other Cu orbitals except the $d_{x^2-y^2}$ ones, will not be suited to describe physics which implies excitations with energy larger than $\approx 1\ eV$. In fact it should be remarked that all the simple model Hamiltonians suggested for the cuprates are not valid when trying to describe the physics at energy scales larger than $1\ eV$. For example the optical spectra or the high energy photoemission lines shapes involve the full complexity of the many orbital case at energy scales above $1\ eV$.

Investigating the relative importance of the various parameters describing the CuO_2 planes [9–11] it was realized that in addition to the Cu on-site Coulomb repulsion ($U_{dd} \approx 8\ eV$) and Cu-O hopping integral ($t_{pd} \approx 1.3 - 1.5\ eV$) the O-O hopping integrals result in a large O $2p$ bandwidth ($W \approx 5.2\ eV$). Even though the Zhang-Rice theory is widely accepted nowadays, probably the most serious critique to it, is the neglect of the O $2p$ band structure. If one takes a different from Zhang and Rice starting point and considers $t_{pd} = 0$, the first hole addition states will belong to the O band. When t_{pd} is switched on, these states will Kondo scatter with the Cu spins and some states will appear at the bottom of the oxygen band. One important question we address here is whether the low-energy electronic states are well separated from the non-bonding oxygen states, so the neglect of the remaining higher energy states and the reduction to a single-band model is possible. This problem was previously considered by Eskes and Sawatzky [12] within an impurity calculation approach, but there both the spatial correlation effects and the dispersion of the low-energy states were neglected.

Other objections to Zhang-Rice assumption were raised by Emery and Reiter[13–15], who showed that in a ferromagnetic background the low-energy states near the Γ point (M in their convention) are an admixture of the Zhang-Rice singlet and the corresponding triplet. This implies a nonzero value for the oxygen spin, and destroys the equivalence of these states to holes. They claim that, even though, as a consequence of the strong Cu-O hybridization low-energy states well separated from the non-bonding oxygen band states appear, this does not necessarily mean that the physics can be reduced to a t-J or to a one-band Hubbard model. Using the DCA technique which provides a means of including all the most important parameters and bands we present here a study of the validity of the single-band approach.

Experimental data show that the phase diagram [16, 17] and other physical characteristics like the density of states (DOS) near the Fermi level of the electron [18] and hole [19] doped materials are profoundly different. There could be multiple reasons responsible for this asymmetry. First, the electron and the hole doped materials are physically different and aside from the CuO_2 planes they contain other elements and have a complex chemical structure. This structural and compositional differences can influence the low-energy physics. Another reason, closely related with the validity of the Zhang-Rice approximation, could be that, unlike the electron-doped materials, the hole-doped materials cannot be described by a single-band Hubbard Hamiltonian. And if this reason does not stand up and Zhang and Rice are correct the motive for the electron-hole asymmetry should come from the different effective parameters which result after the reduction of the multi-band model to a single-band one. Therefore with regard to the electron-hole asymmetry we propose to answer to the following questions:

- Does the physics of a pure CuO_2 plane contain the expected asymmetry or does the origin of the asymmetry in real materials come from other influences?
- Is the Zhang and Rice approximation not valid so that the physics of the hole-doped cuprates cannot be described by a single-band model?
- If Zhang and Rice is correct, what are the effective parameters of the one-band model which are responsible for the electron-hole asymmetry?

6.2 Reduction of Five-Band Hubbard Model to Two-Band Hubbard Model

6.2.1 Derivation of the Five-Band Hubbard Hamiltonian

Restricting ourselves to the energy scale below 1 eV, we can assume that the only relevant Cu degrees of freedom are the $d_{x^2-y^2}$ orbitals, as Eskes *et al.* [9] has shown. They couple with the in-plane oxygen p_x and p_y orbitals. The situation is presented schematically in Fig. 6.1. We work in the hole representation and consider the $Cu(d^{10})O(p^6)$ configuration as the vacuum state. The undoped materials have one hole per CuO_2 unit. The parameters were determined by comparing the Local Density Approximation (LDA) [11, 20], impurity [12] and cluster [9] calculations with experimental data. Their commonly accepted values are around the ones given in the caption of Fig. 6.1. The $d_{x^2-y^2}$ orbitals hybridize via the hopping integral t_{pd} with the p_σ orbitals (drawn with solid line). Aside from the hybridization with the $d_{x^2-y^2}$ orbitals, the p_σ orbitals hybridize via the hopping integral t_{p1} with the nearest-neighbor p_σ and via the hopping integral t_{p2} with the nearest-neighbor p_π orbitals (dashed line). Therefore all degrees of freedom are coupled, and considering that there are two O and one Cu ions per unit cell, a five-band model Hamiltonian (with four O and one correlated Cu bands) is required.

Anticipating the major importance for the low-energy physics of the Cu-O hybridization, we choose the oxygen states basis in the following way. First, on every plaquette of type 1 (see Fig. 6.2), made by four O around a Cu, we construct from the four p_σ orbitals

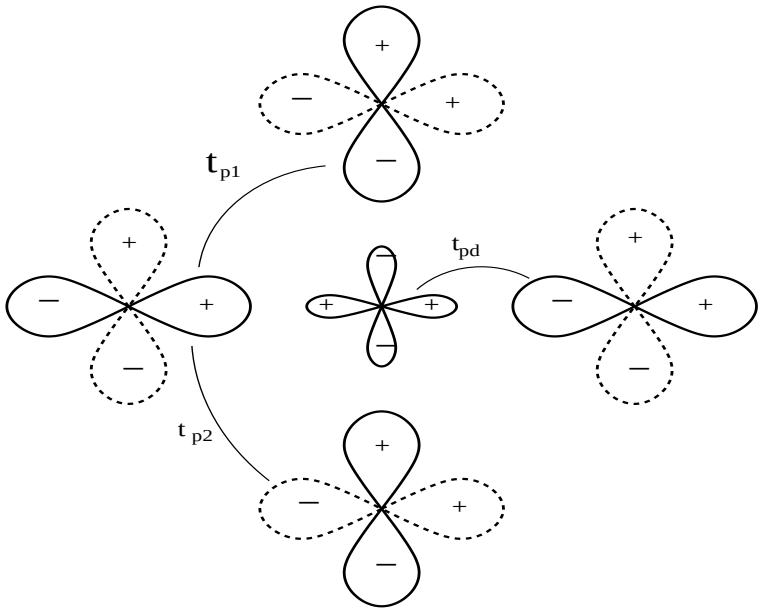

Figure 6.1: *A cooper $d_{x^2-y^2}$ orbital and the four in-plane oxygen p orbitals which surround it. The parameters in the hole representation are: $t_{p1} = -0.65\ eV$, $t_{p2} = 0.35\ eV$, $t_{pd} = -1.3\ eV$, $U_{dd} = 8.8\ eV$, $U_{pp} = 6\ eV$, $U_{pd} = 1.3\ eV$, $E_p - E_d = 3\ eV$.*

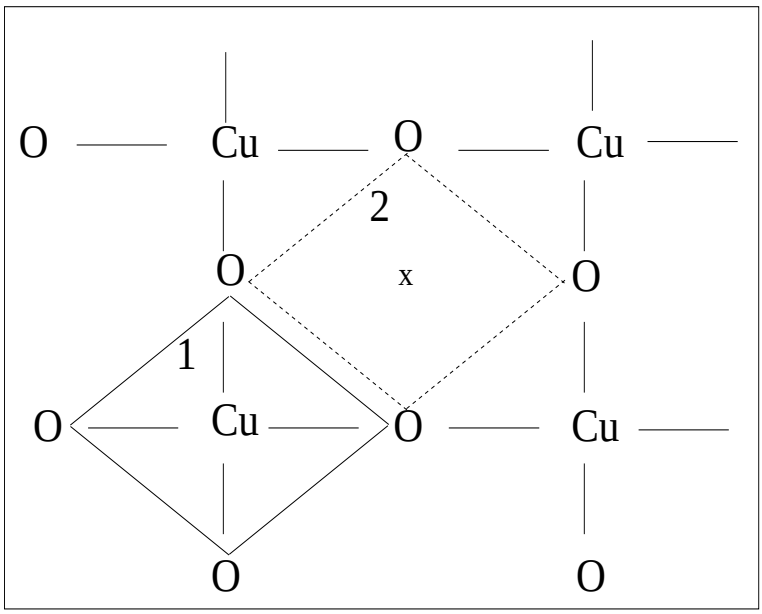

Figure 6.2: *The CuO_2 plane. In constructing the oxygen bands, we consider two kinds of plaquettes. The plaquette of the type* 1 *(solid line) involves the four O ions around a Cu ion and the plaquette of the type* 2 *(dashed line) includes the four O ions around the vacant site denoted with "×"in the figure.*

a linear combination state with $x^2 - y^2$ ($B1$) symmetry, like in Fig. 6.3-a. These states (which we call $B1\sigma$) are the only states which hybridize directly with the $d_{x^2-y^2}$ orbitals, and if the Zhang and Rice theory is correct they should be the only relevant states for the low-energy physics. We use these plaquette states to construct translational invariant (band) states in the same fashion as in Ref. [8]. Afterwards we determine the remaining p_σ and the other two p_π bands. The advantage of this particular choice of the oxygen states basis is that the degrees of freedom considered in Zhang and Rice theory can be separated explicitly from the remaining states.

At site"i" the $B1\sigma$ state (Fig .6.3-a) is:

$$|i_s^{B1\sigma}\rangle = \frac{1}{2}\sum_\delta (-1)^{g(\delta)} |p_{\sigma,s}\rangle_{i,\delta} \tag{6.1}$$

with $g(\delta) = 0$ if $\delta = (0, \frac{1}{2}\hat{x})$ or $\delta = (-\frac{1}{2}\hat{y}, 0)$ and $g(\delta) = 1$ if $\delta = (\frac{1}{2}\hat{y}, 0)$ or $\delta = (0, -\frac{1}{2}\hat{x})$. s is the spin index. The anticommutation relation of these states is

$$\{c_{is}^{B1\sigma}, c_{js'}^{B1\sigma\dagger}\} = \delta_{ss'}(\delta_{ij} - \frac{1}{4}\delta_{<ij>}) \tag{6.2}$$

which implies that the nearest-neighbor states are not orthogonal. Here $c_{is}^{B1\sigma}$ ($c_{is}^{B1\sigma\dagger}$) is the annihilation (creation) operator of a $B1\sigma$ oxygen hole with spin s and at site "i". From these local states we construct orthogonal Bloch states,

$$|k_s^{B1\sigma}\rangle = \frac{1}{\beta(k)}\frac{1}{N}\sum_i |i_s^{B1\sigma}\rangle \; e^{-ikr_i} \tag{6.3}$$

were $\beta(k)$ is a normalization factor consequence of the nearest-neighbor states nonorthogonality (Eq. 6.2)

$$\beta(k) = [\sin^2(k_x/2) + \sin^2(k_y/2)]^{1/2} \tag{6.4}$$

If we define

$$|p_{\sigma,s}\rangle_{kx} = \frac{1}{N}\sum_i |p_{\sigma,s}\rangle_{ix} \; e^{-ikr_i} \tag{6.5}$$

where $|p_{\sigma,s}\rangle_{ix}$ is the p_σ orbital along x direction at position "r_i" and analogous

$$|p_{\sigma,s}\rangle_{ky} = \frac{1}{N}\sum_i |p_{\sigma,s}\rangle_{iy} \; e^{-ikr_i} \tag{6.6}$$

with $|p_{\sigma,s}\rangle_{iy}$ being the p_σ orbital along y direction at position "r_i", we obtain from Eq. 6.3 and Eq. 6.1

$$|k_s^{B1\sigma}\rangle = \frac{i}{\beta(k)}[\sin(k_x/2) \; |p_{\sigma,s}\rangle_{kx} - \sin(k_y/2) \; |p_{\sigma,s}\rangle_{ky}] \tag{6.7}$$

Now it is easy to see that the other p_σ band is defined by the states

$$|k_s^{B2\sigma}\rangle = \frac{i}{\beta(k)}[\sin(k_y/2) \; |p_{\sigma,s}\rangle_{kx} + \sin(k_x/2) \; |p_{\sigma,s}\rangle_{ky}] \tag{6.8}$$

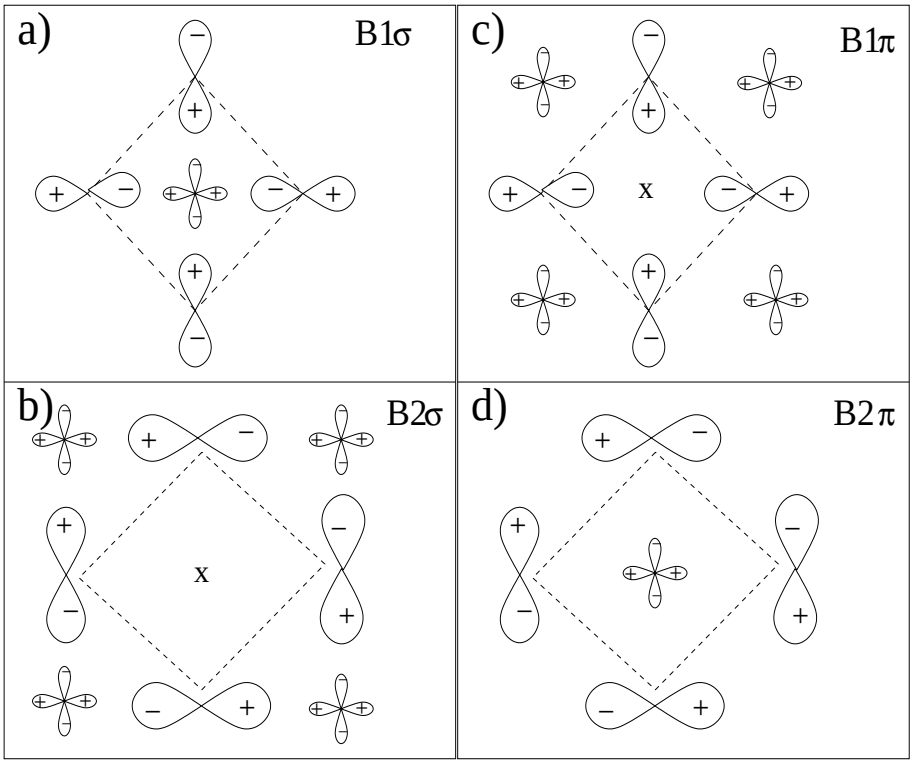

Figure 6.3: *a) $B1\sigma$ state. Combination with x^2-y^2 ($B1$) symmetry of the p_σ orbitals on a plaquette of type* 1. *b) $B2\sigma$ state. Combination with xy ($B2$) symmetry of the p_σ orbitals on a plaquette of type* 2. *c) $B1\pi$ state. Combination with x^2-y^2 ($B1$) symmetry of the p_π orbitals on a plaquette of type* 2. *c) $B2\pi$ state. Combination with xy ($B2$) symmetry of the p_π orbitals on a plaquette of type* 1.

which are orthogonal on $|k_s^{B1\sigma}\rangle$ states.
Going back from momentum to site representation, we find that the $|k_s^{B2\sigma}\rangle$ states are obtained by taking a linear combination with xy ($B2$) symmetry of the four O p_σ orbitals around a plaquette of type 2 (Fig. 6.3-b), and afterwards constructing Bloch translational invariant states.

We construct the remaining two p_π bands in a similar way. First one can notice that the situation is identical with the previous one (the one regarding the p_σ bands construction) if the Cu sites are interchanged with the vacant sites denoted by "×"in Fig. 6.2 (or equivalently if the plaquette 1 is interchanged with the plaquette 2). The $B1\pi$ band is obtained from the states with x^2-y^2 symmetry formed by the four O p_π orbitals on a plaquette of type 2 (Fig. 6.3-c), and the $B2\pi$ band from states with xy symmetry formed by the four O p_π orbitals on a plaquette of type 1 (Fig. 6.3-d).

$$|k_s^{B1\pi}\rangle = \frac{i}{\beta(k)}[\sin(k_x/2)\ |p_{\pi,s}\rangle_{kx} - \sin(k_y/2)\ |p_{\pi,s}\rangle_{ky}] \tag{6.9}$$

$$|k_s^{B2\pi}\rangle = \frac{i}{\beta(k)}[\sin(k_y/2)\ |p_{\pi,s}\rangle_{kx} + \sin(k_x/2)\ |p_{\pi,s}\rangle_{ky}] \tag{6.10}$$

with

$$|p_{\pi,s}\rangle_{kx} = \frac{1}{N}\sum_i |p_{\pi,s}\rangle_{ix}\ e^{-ikr_i} \tag{6.11}$$

$$|p_{\pi,s}\rangle_{ky} = \frac{1}{N}\sum_i |p_{\pi,s}\rangle_{iy}\ e^{-ikr_i} \tag{6.12}$$

The Hamiltonian written in the above constructed basis (which consists of the five bands, namely d, $B1\sigma$, $B2\sigma$, $B1\pi$ and $B2\pi$) is

$$H = H_0 + H^U \tag{6.13}$$

H_0 is the one-particle part of the Hamiltonian which describes the bands dispersion

$$H_0 = \sum_{ks} H_{ks} \tag{6.14}$$

with

$$H_{ks} = \left(\begin{array}{ccccc} d_{ks}^{\dagger} & c_{ks}^{B1\sigma\dagger} & c_{ks}^{B2\sigma\dagger} & c_{ks}^{B1\pi\dagger} & c_{ks}^{B2\pi\dagger} \end{array}\right) \times$$

$$\times \begin{pmatrix} E_d(k) & V_{pd}(k) & 0 & 0 & 0 \\ V_{pd}(k) & E_1(k) & V_{p1}(k) & V_{p2}(k) & 0 \\ 0 & V_{p1}(k) & E_2(k) & 0 & V_{p2}(k) \\ 0 & V_{p2}(k) & 0 & E_1(k) & V_{p1}(k) \\ 0 & 0 & V_{p2}(k) & V_{p1}(k) & E_2(k) \end{pmatrix} \begin{pmatrix} d_{ks} \\ c_{ks}^{B1\sigma} \\ c_{ks}^{B2\sigma} \\ c_{ks}^{B1\pi} \\ c_{ks}^{B2\pi} \end{pmatrix} \tag{6.15}$$

and

$$E_d(k) = E_d \tag{6.16}$$

$$E_1(k) = E_p + 8t_{p1}\frac{1}{\beta(k)^2}\sin^2(k_x/2)\sin^2(k_y/2) \tag{6.17}$$

$$E_2(k) = E_p - 8t_{p1}\frac{1}{\beta(k)^2}\sin^2(k_x/2)\sin^2(k_y/2) \tag{6.18}$$

$$V_{pd}(k) = 2t_{pd}\beta(k) \tag{6.19}$$

$$V_{p1}(k) = 4t_{p1}\frac{1}{\beta(k)^2}[\sin^2(k_x/2) - \sin^2(k_y/2)]\sin(k_x/2)\sin(k_y/2) \tag{6.20}$$

$$V_{p2}(k) = -4t_{p2}\cos(k_x/2)\cos(k_y/2) \tag{6.21}$$

If $t_{pd} = 0$ the oxygen bands with the same symmetry would be degenerate, as can be seen from Eq. 6.15. The bottom of the oxygen band has $B1$ symmetry and contains both $B1\sigma$ and $B1\pi$ states. The mixing of $B1\sigma$ and $B1\pi$ given by Eq. 6.21 is strong, modifying significantly the DOS of the noninteracting $B1$ bands. When t_{pd} is switched

on, the $B1\sigma$ band mixes with the d one, and bonding low-energy states with mainly $B1\sigma$ and d character will appear. From the oxygen degrees of freedom in order of importance, with respect to the low-energy physics, the $B1\pi$ are the next after the $B1\sigma$ states, and there are no priori reasons to neglect these states. However these p_π orbitals are more important than the p_σ ones which enter in the $B2\sigma$ band.

H^U contains the Coulomb repulsion terms

$$H^U = U_{dd}\sum_i n_{di\uparrow}n_{di\downarrow} + U_{pp}\sum_{i,\alpha,\alpha',s,s'} n_{pi\alpha s}n_{pi\alpha' s'} + U_{pd}\sum_{i,s,s',\alpha} n_{pi\alpha s}n_{dis'} \tag{6.22}$$

with α and s being the oxygen band and respectively the spin index. The first term of Eq. 6.22 is the Coulomb repulsion between two holes on a $d_{x^2-y^2}$ orbital. The second term is the Coulomb repulsion between two holes on the same O and the third represents the repulsion between one O hole and one nearest-neighbor Cu hole. Even if theoretically it is possible to treat within the DCA framework all these Coulomb terms, practically this is unfeasible at the moment because of the limited computer resources available. However, for the physical regime relevant for the high T_c superconductors, the occupation of the oxygen ions is rather small (below 30%), therefore we assume that treating the last two terms of Eq. 6.22 in a mean-field way is pretty good. The mean-field approach results in an increase of the charge transfer parameter $\Delta = E_p - E_d$ by $U_{pp}\frac{\overline{n}_p}{2} + U_{pd}\overline{n}_d$ so

$$\Delta^{eff} = E_p - E_d + U_{pp}\frac{\overline{n}_p}{2} + U_{pd}\overline{n}_d \tag{6.23}$$

Starting with the parameters given in Fig. 6.1 and approximating the oxygen occupation with $\overline{n}_p \approx 0.3$ we obtain a value of $\Delta^{eff} = 4.8\ eV$. We did not find dramatic changes in the physics with small modifications in Δ, therefore we are going to keep the value of Δ constant for all doping levels.

To conclude this section, our model Hamiltonian is given by the Eq. 6.13 with $U_{pp} = 0$, $U_{pd} = 0$ and $\Delta = E_p - E_d = 4.8\ eV$. The other parameters value is given in Fig. 6.1's caption.

6.2.2 DCA Applied to the Five-Band Hubbard Model

It is straightforward to apply the DCA technique to our five-band model. When $U = 0$, the Green's function is defined by

$$G_{0s}^{-1}(k, i\omega) = i\omega - H_{ks} \tag{6.24}$$

When the Coulomb interaction is switched on, the Green's function is obtained from Eq. 6.24 by replacing E_d with $E_d + \Sigma(K, i\omega)$. This is a 5×5 matrix which can be easily inverted analytically. During the coarse-graining process, $G(k, i\omega)$ is needed in all k and ω points, therefore, for the computation speed reasons it is important to have an analytical expression of the Green's function. We used *Mathematica* for the analytical inversion. The calculation of the cluster excluded Green's function $\mathcal{G}$ implies only the d part of the coarse-grained $\bar{G}$

$$\mathcal{G}^{-1}(K, i\omega) = \bar{G}_{dd}^{-1}(K, i\omega) + \Sigma(K, i\omega) \tag{6.25}$$

and from this point the calculation of $\Sigma(K, i\omega)$ and $\Gamma_{Q,i\nu}(K, i\omega; K', i\omega')$ is identical with the one presented in Chap. 5.

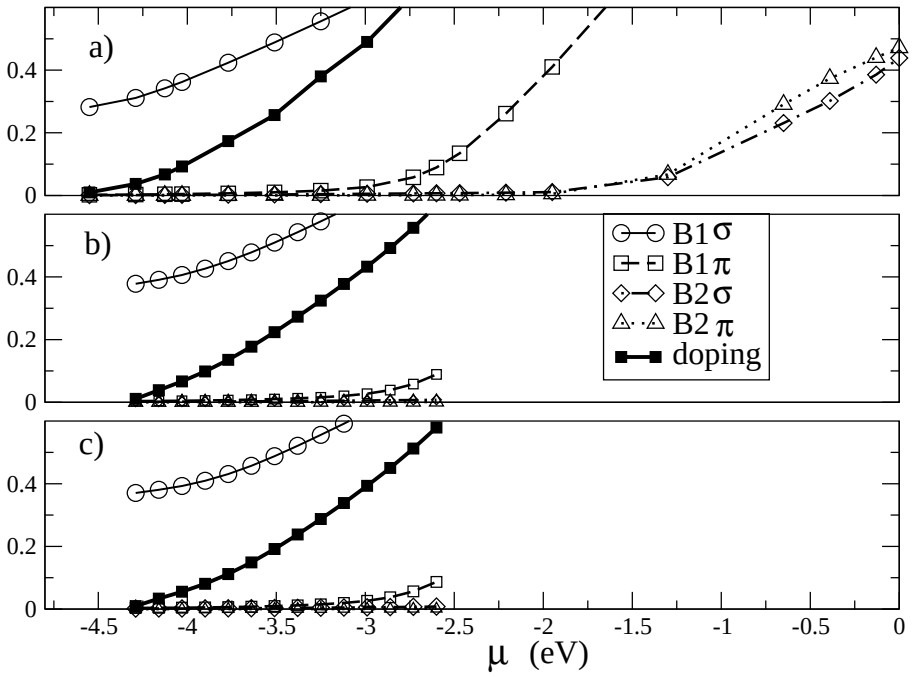

Figure 6.4: *Occupation of the four oxygen bands versus chemical potential at* $T = 1885\ K$. *a)* $\Delta = 4.8eV, U = 8.8eV$. *b)* $\Delta = 3.5eV, U = 8.8eV$. *c)* $\Delta = 3.5eV, U = 11eV$. *The solid line represents the hole doping. Notice that up to 40% doping the occupation of the oxygen bands which do not hybridize directly with Cu is less than 1%. The second oxygen band which starts to populate when doping increases above 40% is* $B1\pi$.

6.2.3 Comparison of Five-Band and Two-Band Hubbard Models

In this section we study the importance of the different oxygen degrees of freedom by calculating the five-band Hubbard model properties with the DCA technique. An indication of the relevance to the low-energy physics of the different oxygen bands would be given by their occupation number upon doping. Finally, we compare the five-band model properties with a reduced two-band model (which we suspect to approximate the low-energy physics) ones, and decide about the validity of this approximation. In the DCA algorithm we take a cluster of 2×2 Cu ions, which we believe is large enough to capture qualitatively the essential physics of cuprates.

Upon hole doping, the extra holes go primarily on the oxygen. We plotted in Fig. 6.4 the oxygen bands occupation number as a function of the chemical potential. Notice that increasing the chemical potential is equivalent to increasing the hole doping. It can be seen that only one oxygen band, the $B1\sigma$, is populated up to 40% hole doping, the other three oxygen bands ($B2\sigma$, $B1\pi$, $B2\pi$) being very sparsely occupied (less than 1%) even at high temperature (1885K). When the temperature is lowered their occupation number is even less. The realistic parameters are the ones in Fig. 6.4-a, but our conclusion holds even for different values of U and Δ, as long as the Cu-O hopping t_{pd} is significant, as can be seen form Fig. 6.4-b and Fig. 6.4-c. As we have discussed earlier, only the $B1\sigma$ band directly hybridizes with Cu. This hybridization is very strong and not only due to the large t_{pd} but mainly because of the symmetry and phase coherence between the $d_{x^2-y^2}$

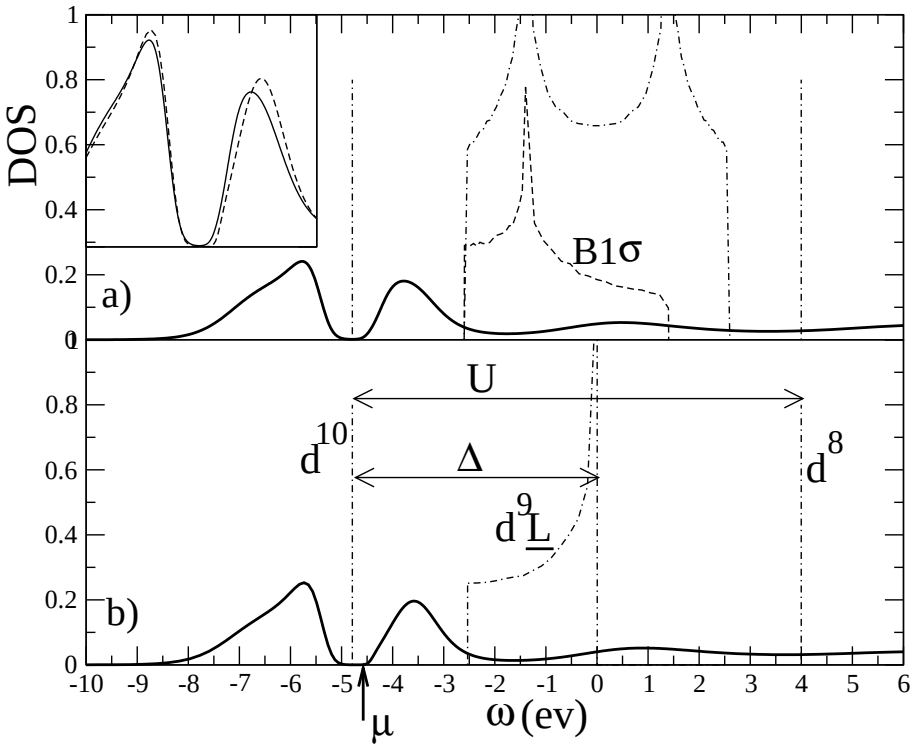

Figure 6.5: *Density of states of the five-band Hubbard a) and the two-band Hubbard b) model. The doted-dashed line represents the total DOS before the Cu-O hopping t_{pd} is switched on. The solid line is the d part of the DOS calculated with MEM at $T = 837$K in the undoped region, $\mu = -4.55\ eV$. Inset: Comparison of the low-energy partial d DOS between five-band (solid line) and two-band (dashed line) models.*

and $B1\sigma$ states (at the (π, π) point the hybridization matrix element is $2\sqrt{2}t_{pd} \approx 3.7eV$). As a consequence, low-energy states with the energy well enough below the energy of the non-bonding oxygen states and with only d and $B1\sigma$ character will appear. The other three oxygen bands do not couple directly with Cu and they do not enter in the formation of the low-energy states.

The density of states (DOS) in the undoped case can be seen in Fig. 6.5-a. When $t_{pd} = 0$ the hole addition states have pure oxygen character. Their energy is $\Delta - W/2$. The DOS for $t_{pd} = 0$ is shown with dash-dotted line. The $B1\sigma$ part of the oxygen DOS is shown with dashed line. As long as $t_{pd} = 0$ the $B1\sigma$ density of states is degenerate with the $B1\pi$ one. The higher in energy part of the oxygen DOS is made by the degenerate $B2\sigma$ and $B2\pi$ bands. When t_{pd} is switched on, the first hole addition states have a mixed character (d and p) and are pushed to lower energies. The partial d DOS of these states is drawn with the solid line, and was obtained using Maximum Entropy Method (MEM)[21] for the analytic continuation of the QMC data to real frequencies.

The $B1\sigma$ density of states is strongly influenced by the hybridization of the $B1\sigma$ states with the other oxygen states, especially with the ones belonging to $B1\pi$ band. Therefore, even though the low-energy states have only d and $B1\sigma$ character, the other oxygen bands, non-directly hybridizing with Cu, have an indirect influence. In order to estimate this

	two-band Hubbard	five-band Hubbard	relative deviation	μ
$\overline{n}_p$	0.2650	0.2722	2.5%	
$\overline{n}_d$	0.7428	0.7376	0.7%	
χ^c_{charge}	0.2117	0.2206	4%	-4.55 eV
$\langle(n_{di\uparrow} - n_{di\downarrow})^2\rangle$	0.7328	0.7273	0.8%	
$T * \chi_{local}$	0.4482	0.4390	2%	
$\overline{n}_p$	0.4448	0.4723	5%	
$\overline{n}_d$	0.8094	0.8074	0.2%	
χ^c_{charge}	0.2290	0.2288	0.3%	-3.51 eV
$\langle(n_{di\uparrow} - n_{di\downarrow})^2\rangle$	0.7433	0.7367	0.8%	
$T * \chi_{local}$	0.3377	0.3116	7%	

Table 6.1: *Comparison of different cluster quantities calculated for the two-band model and the the five-band model at* $T = 1885K$.

influence, we compare the properties of the five-band Hubbard model with the ones of a two-band Hubbard model which considers only the Cu $d_{x^2-y^2}$ and the oxygen $B1\sigma$ states. The two-band Hubbard Hamiltonian can be obtained from the five-band Hubbard one (Eq. 6.13) taking $V_{p1} = 0$ and $V_{p2} = 0$ in Eq. 6.15. This leads to

$$H = \sum_{ks} E_{p1}(k) c^\dagger_{ks} c_{ks} + E_d d^\dagger_{ks} d_{ks} + V_{pd}(k)(d^\dagger_{ks} c_{ks} + h.c.) + U \sum_i n_{di\uparrow} n_{di\downarrow} \tag{6.26}$$

where now $c^\dagger$ (c) represents the $B1\sigma$ hole creation (annihilation) operator.
The two-band Hubbard model density of states is shown in Fig. 6.5-b. The $B1\sigma$ oxygen DOS looks very different from the five-band Hubbard model one. Nevertheless, we found that the low-energy DOS is very similar in both cases. The difference between them can be seen in the inset of Fig. 6.5. In the five-band model the gap is a little smaller and the first hole addition states are "pushed" a little further from the oxygen band. This presumably is due to the fact that the oxygen DOS, which mixes with Cu, is larger at the bottom of the oxygen band (where the hybridization is the strongest). However, the difference between the two cases is small and does not change the qualitative physics. Even the quantitative physics differs very little, as can be noticed from Table 6.1, where a comparison between different cluster quantities calculated for the two-band and for the five-band Hubbard models is presented. $\overline{n}_p$ and $\overline{n}_d$ are the $B1\sigma$ and respectively the Cu occupation number, χ^c_{charge} is the charge susceptibility measured on the cluster, $\langle(n_{di\uparrow} - n_{di\downarrow})^2\rangle$ is the unscreened moment on a Cu site and

$$T * \chi_{local} = \frac{T}{N} \sum_i \int_0^\beta \langle S^-_i(\tau) S^+_i(0)\rangle d\tau, \tag{6.27}$$

with S_i being the Cu spin operator at site "i', is the screened Cu moment. The difference between the two cases is only a few percent.

So far we can conclude that for the low-energy physics the Cu-$B1\sigma$ hopping integral is the most important one, much more important than the hopping terms which determine the oxygen band dispersion. As a consequence of this strong Cu-$B1\sigma$ mixing, the low-energy states are well stabilized with respect to the initial (i.e. when $t_{pd} = 0$) oxygen band and have only $d_{x^2-y^2}$ and $B1\sigma$ character. The other than $B1\sigma$ oxygen bands can be neglected to a a very good approximation, and a two-band Hubbard model is well suited for describing the low-energy physics of the CuO_2 planes.

At the end of this section we want to make a remark about the importance of the $B1\pi$ band. As can be seen from Fig. 6.4, this is the first oxygen band after the $B1\sigma$ which starts to populate upon hole doping. Therefore, if for some reasons, like describing experiments which explore high energy excitations (of order of $1 - 2\ eV$), a three-band model is necessary, we believe that it should contain all the bands with $x^2 - y^2$ symmetry, i.e. $d_{x^2-y^2}$, $B1\sigma$ and $B1\pi$, quite opposite to what is commonly proposed, namely a three-band model with the $d_{x^2-y^2}$ and the p_σ ($B1\sigma$ and $B2\sigma$) bands.

6.3 Two-Band Hubbard Model

6.3.1 Phase Diagram and Other Properties

In this section we present the DCA calculation of the two-band Hubbard model. The Hamiltonian is given by Eq. 6.26 and according to the conclusions of Section 6.2 we assume it describes very well the low-energy physics of the CuO_2 planes. Due to the large computational effort, our cluster is still the smallest one which allows an explicit treatment of the short-range spatial correlation and permits d-wave pairing, and consists of four Cu ions. As we are going to show, the calculation on even this small cluster, captures much of

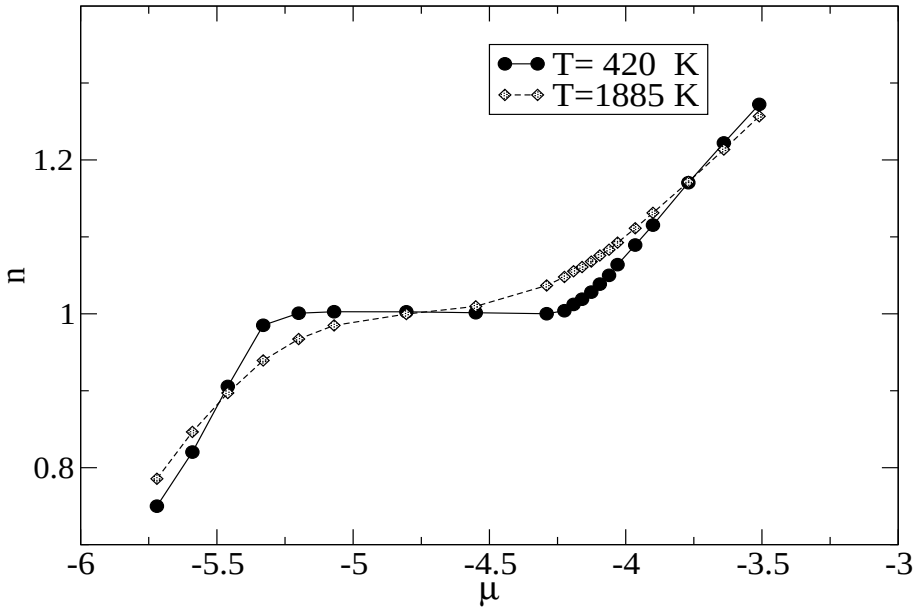

Figure 6.6: *The hole occupation number n, versus chemical potential μ.*

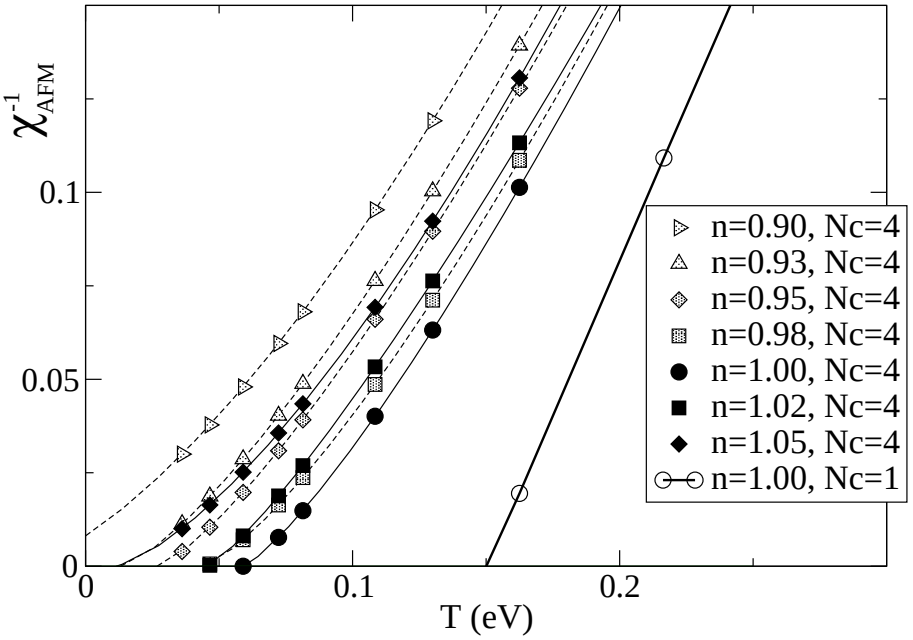

Figure 6.7: *Inverse of the antiferromagnetic susceptibility χ^{-1}_{AFM} versus temperature calculated for $N_c = 4$ at different hole densities and for $N_c = 1$ at $n = 1.00$.*

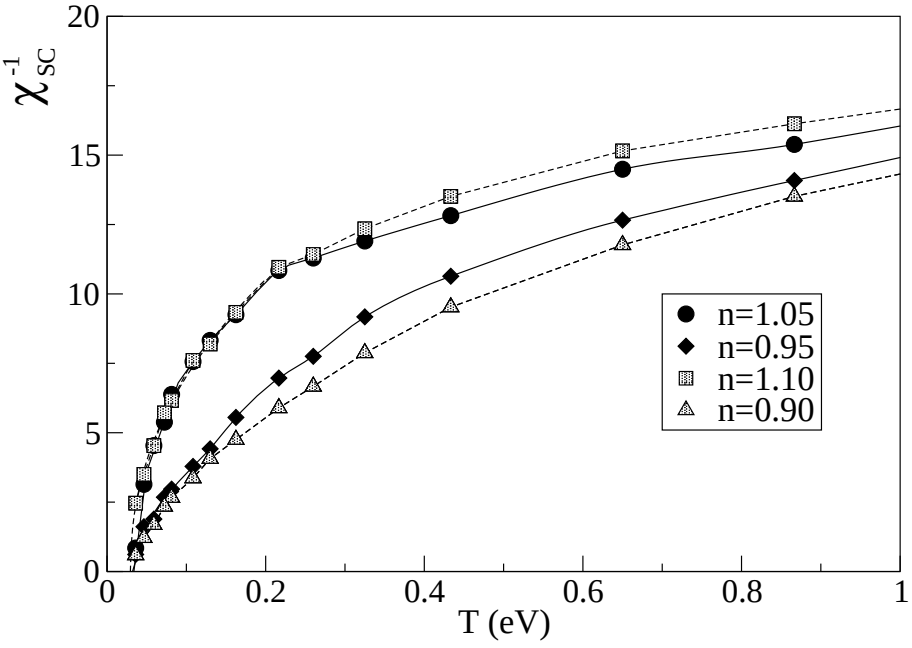

Figure 6.8: *Inverse of the d-wave pairing susceptibility χ^{-1}_{SC} versus temperature for different hole densities.*

the essential physics of cuprates, the phase diagram resembling the generic phase diagram of high T_c materials. We found regions characterized by antiferromagnetism, pseudogap and d-wave superconductivity for both electron and hole doped systems.

The undoped system is an insulator. This can be seen in Fig 6.5-b, where at $T = 837$ K the DOS exhibits a gap of 0.6 eV. When the temperature is lowered, the value of the gap increases. Based on the results presented in Fig 6.6, where the hole occupation number as a function of chemical potential is shown, we estimate a gap of $\approx 1.1\ eV - \ 1.2eV$ at $T = 0$ K. This gap is smaller than the real gap found in the undoped cuprates superconductors ($\approx 1.5\ eV - 2\ eV$), but this is mainly due to our small cluster choice ($N_c = 4$). We expect an increase in the value of gap for larger clusters, similar to what was found in the one-band Hubbard model calculation [22].

The phase diagram was determined by calculating the relevant susceptibilities. A divergence in the susceptibility function at a certain temperature indicates that the system becomes instable, and a phase transition takes place. We calculated a large number of susceptibilities which are relevant for spin, charge and superconducting ordering, both at the center and at the corner of the Brillouin Zone.

In the undoped regime and at small doping (both with holes and with electrons) we found the antiferromagnetic susceptibility to diverge, meaning that a transition to an antiferromagnetic state takes place over there. In Fig. 6.7 we show the inverse of the antiferromagnetic susceptibility χ^{-1}_{AFM} as a function of temperature, at different doping concentrations. The transition temperature (the Neel temperature) T_N is the temperature where χ^{-1}_{AFM} reaches the value zero. In the same figure, for comparison, we also show the DMFT result (i.e. $N_c = 1$ case). The non-local fluctuations allowed in DCA reduce the value of the Neel temperature and make the transition critical exponent γ larger than 1 (always $\gamma = 1$ in DMFT).

We computed different pairing susceptibilities, with different symmetries, as s-wave, p-wave and d-wave of both odd and even frequency and we looked for paring at both the zone center and zone corner. From all of these only the d-wave pairing at the zone center diverges. In Fig. 6.8 we show the inverse of the d-wave pairing susceptibility χ^{-1}_{SC} versus temperature. The d-wave superconductivity starts at very low doping ($\approx 1\%$) and persists up to $\approx 24\%$ electron doping and $\approx 30\%$ hole doping. For the superconducting transition the critical exponent γ is smaller than 1.

Using the Maximum Entropy Method we calculated the single particle density of states at different doping concentrations. The total d part of the low-energy DOS at 5% doping is shown with thick solid line in Fig. 6.9, for both the electron and hole doped case. Below a characteristic temperature T^*, larger than the superconducting critical temperature T_c, we notice a suppression of states at the chemical potential, which indicates the presence of a pseudogap. The pseudogap increases decreasing temperature. Since the MEM calculation of the DOS becomes computationally extremely expensive at lower temperatures, we plotted the DOS at the highest temperature where the pseudogap was clearly seen. This temperature does not necessarily have to be the same for the electron and hole doped case (see Section 6.3.2 for electron-hole asymmetry discussion).

The uniform spin susceptibility which is shown in the upper part in Fig. 6.10 also displays evidence of the pseudogap. At the pseudogap temperature T^* the spin excitations are suppressed and a downturn in the susceptibility function is seen. The suppression

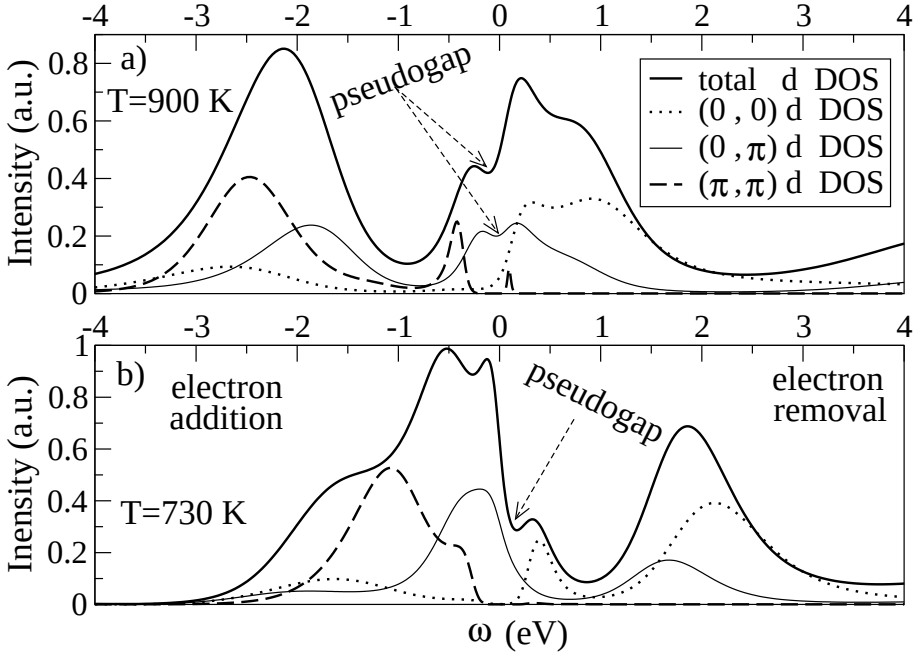

Figure 6.9: *a) Total d DOS and coarse-grained K dependent d DOS at 5% doping. a) hole doping case. b) electron doping case.*

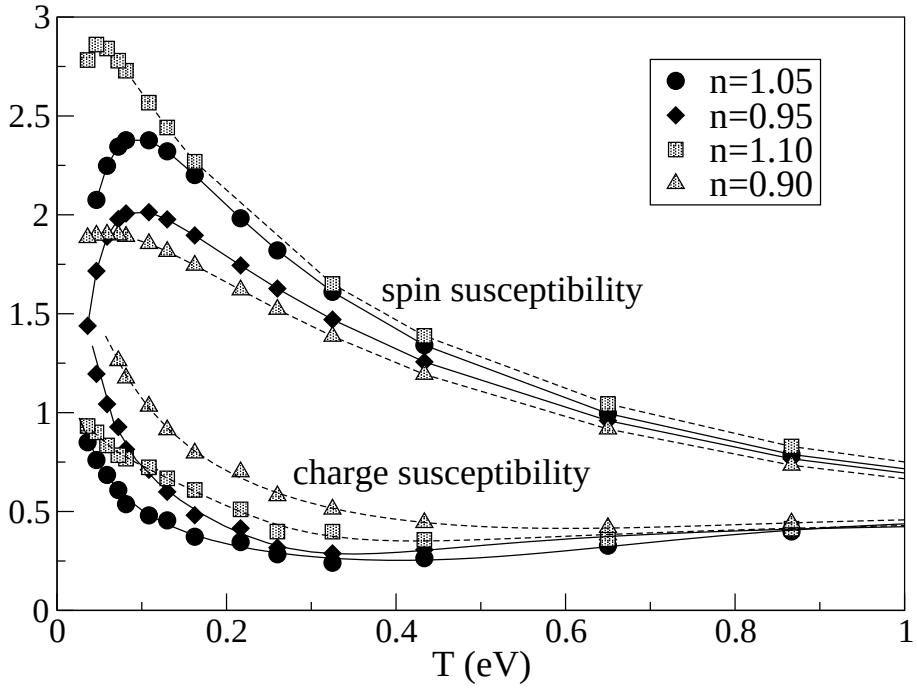

Figure 6.10: *Uniform spin (upper part) and charge (lower part) susceptibilities versus temperature for different hole densities.*

of the spin excitations below T^* was seen early on in the NMR experiments and was associated with the pseudogap [23–25]. An interesting feature is that the uniform charge susceptibility (shown in the lower part of Fig. 6.10) is strongly enhanced in the underdoped region below the same T^*, showing that in the pseudogap phase the spin and the charge degrees of freedom behave profoundly differently, i.e. the former are suppressed and the later are enhanced.

The phase diagram calculated for $N_c = 4$, is shown in Fig. 6.11. At small doping, the overlap of the antiferromagnetic phase and the superconducting one does not necessarily mean that the two phases coexists. Because our algorithm forces the system to be always in a paramagnetic phase, it merely states that if the antiferromagnetic phase is suppressed for some reasons (e.g. due to impurities or long-range interactions), a transition to a superconducting state at a smaller temperature is possible. The phase diagram resembles the generic phase diagram of cuprates, except the fact that superconductivity phase exists at very small doping concentrations and the maximum T_c is around 5% doping (and not around 15%, as in real materials). We believe that this is a consequence of our small cluster choice, and a more realistic phase diagram would correspond to larger clusters, as single-band Hubbard model calculation shows (see Chap. 7). Unfortunately, due to the limited computational resources available we could not do calculations on larger clusters for the two-band model.

Because of the large $Cu-O$ hybridization the system is strongly covalent. For example in the undoped regime the Cu occupation number is only $\approx 73\%$. This is in agreement with cluster [9] and impurity [12] calculations and also with NMR measurements [26, 27]. The $Cu-O$ hybridization (Eq. 6.19) is strongly k dependent, its value taking values from $2\sqrt{2}t_{pd}$ at (π, π) point to zero at $(0, 0)$ point in the Brillouin Zone (BZ). Consequently the system exhibits a slightly doping dependent covalency. This is shown in Fig. 6.12-a where the Cu occupation number versus hole density is plotted. A constant covalency, equal to the one in the undoped regime (i.e. 0.73 Cu holes and 0.27 O holes per site), would correspond to the dashed line. It can be noticed that, for the electron doped regime, the Cu hole occupation number is decreasing faster than the hole concentration, which indicates an increasing covalency with increasing the electron doping. This is because at large electron doping, i.e. when the filling with holes of CuO_2 plane is small, the effective hybridization is a result of a large $V_{pd}(k)$ in the BZ. Increasing the number of holes, the BZ starts to fill up and a smaller $V_{pd}(k)$ will be responsible for the hybridization, therefore the covalency is decreasing. For the hole doped regime, the extra holes go primarily on the oxygen band, and the system becomes more complicated. In Fig. 6.12-a the unscreened moment on Cu orbitals is also shown. It is defined as in the Figure 6.12's caption and can be written also as

$$\mu^2 = n_d - 2\langle n_{di\uparrow} n_{di\downarrow} \rangle \tag{6.28}$$

The difference between n_d and μ^2 is a measure of the double occupancy with holes of Cu sites. In the electron doped regime the double occupancy is very small, but it increases substantially in the hole doped regime, which indicates that the low-energy hole addition states contain double occupied Cu configurations in a significant measure. An important effect of the extra holes is to screen the spins on the Cu sites, as can be seen in Fig. 6.12-b.

In the Zhang- Rice scenario an extra hole perfectly screens one spin on Cu forming a strongly bound on-site singlet which would contain a significant amount of the double

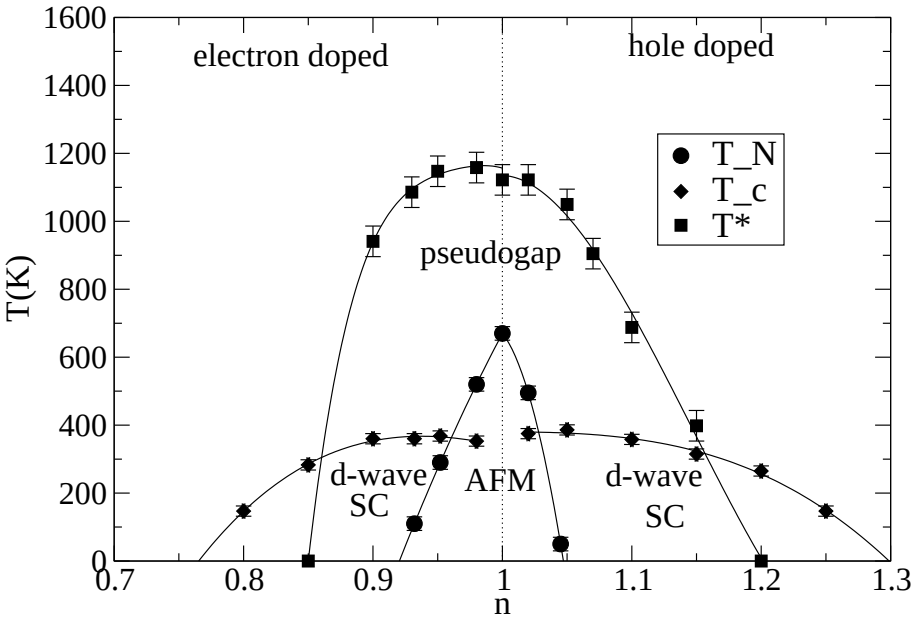

Figure 6.11: *Two-band Hubbard model phase diagram.*

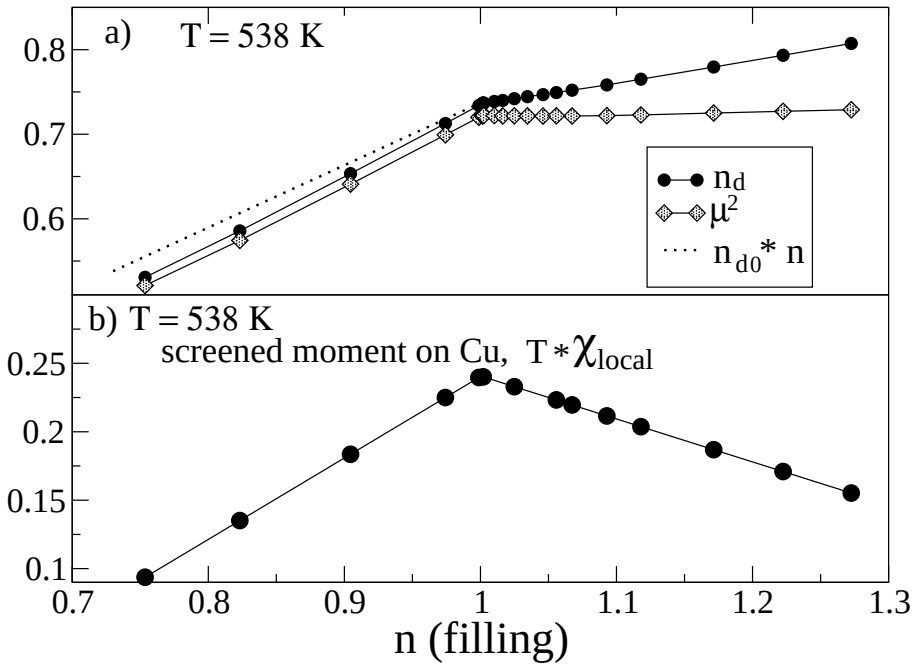

Figure 6.12: *a) The Cu occupation number, n_d, the unscreened Cu moment, $\mu^2 = \langle (n_{di\uparrow} - n_{di\downarrow})^2 \rangle$ versus hole filling. b) The screened Cu moment, $T * \chi_{local}$ (Eq. 6.27) versus hole filling.*

occupied Cu configuration. So, our results do not contradict the Zhang and Rice theory, but also do not exclude other scenarios where the extra holes form more complicated bound states which involve more than one Cu spin. Quantitative analysis based on the amount of screening as function of hole doping cannot give an answer to the validity of Zhang and Rice assumption, because, aside from the screening due to the oxygen holes, there are also non-local processes which contribute to the screening of Cu moments (for example the possible formation of inter-site spin singlets associated with the Resonance Valence Bond scenario). Therefore, in order to decide about the validity of Zhang and Rice approximation, in Sec. 6.4 we are going to take another approach, making a comparison of the single-particle and the two-particle properties of the two-band and single-band Hubbard models.

6.3.2 Electron-Hole Asymmetry

The DCA results show that the two-band Hubbard model is not symmetric with respect to electron and hole doping. The asymmetry is seen in the phase diagram, in the one-particle spectral functions and in the susceptibility functions.

Looking at the phase diagram (Fig. 6.11) it can be seen that, comparative to the hole doped regime, the antiferromagnetism in the electron doped regime persists up to a larger critical doping. With respect to the d-wave superconductivity phase the situation is quite opposite, in the electron doped case the superconductivity being destroyed at smaller critical doping. These features are in qualitative agreement with experimental findings (see Fig. 1.3). The pseudogap temperature measured as the temperature where the spin excitations are suppressed also shows strong asymmetry, but one has to be careful here because a larger T^* in the electron-doped case does not necessarily mean that the pseudogap is stronger (i.e. more developed), as we are going to discuss in the last paragraph of this section.

Recent photoemission experiments on electron-doped materials [18] show that the angle resolved photoemission spectra (ARPES) are profoundly different from the ones corresponding to hole-doped materials. The 2×2 cluster limits us to coarse the Brillouin zone in four cells around K=$(0,0), (0,\pi), (\pi,0)$ and (π,π) (see Fig. 6.13), and approximate the lattice self-energy with $\Sigma(K,\omega)$. Due to this rough coarse-graining the comparison to ARPES is not possible aside from gross features, like pseudogap, occurring over a wide range of k space. With respect to the pseudogap, an important difference between the underdoped electron and the underdoped hole doped regimes can be seen in Fig. 6.9. There, besides the total d states DOS we also show the d coarse-grained momentum dependent DOS, which would correspond to the average over all k belonging to a coarse-grained cell of single particle spectra $A(k,\omega)$. Unlike the total DOS which looks qualitatively similar and displays a pseudogap at the chemical potential, the K dependent DOS are very different. In the hole doped case the pseudogap appears around $(0,\pi)$ as can be seen form the thin-solid line plot in Fig. 6.9-a. For the electron doped case we did not detect any suppression of states around $(0,\pi)$ (see the thin-solid line plot in Fig. 6.9-b) even though the pseudogap is clearly present in the total DOS. These features are in agreement with experimental data. At small doping, the ARPES of the normal state hole-doped systems exhibits well defined quasiparticle peaks around the $(\pi/2,\pi/2)$ point

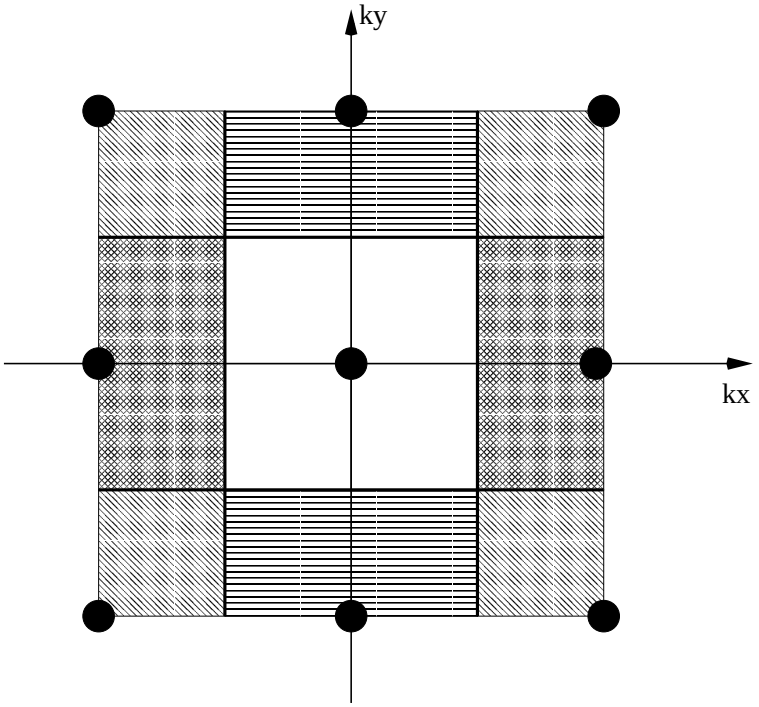

Figure 6.13: *Coarse-graining of the Brillouin Zone in four cells ($N_c = 4$) around K=$(0,0),(0,\pi),(\pi,0)$ and (π,π).*

in Brillouin Zone, and broad gapped states around the $(0,\pi)$ and $(\pi,0)$ points [19]. In the electron-doped samples, the ARPES measurements show Fermi surface pockets around $(0,\pi)$ point (and around the symmetry related $(\pi,0)$ point), and gapped states near the $(\pi/2,\pi/2)$ point [18]. With DCA the presence of the pseudogap at $(\pi/2,\pi/2)$ for the electron doped system can by only checked by increasing the cluster size, and some results regarding this matter are presented in the Chapter 7.

As can be seen from Fig. 6.10 and Fig. 6.8 the electron and the hole-doped spin, charge and pairing susceptibility functions are also different both for the divergence temperatures and the temperature and doping dependence. In the hole doped case, the spin susceptibility at the pseudogap temperature T^* strongly increases with doping unlike in the electron doped case where it decreases upon doping. At the same doping the hole doped spin susceptibility is much larger than the electron doped one. For the hole doped case the downturn in the susceptibility (which defines T^*) is sharp and moves to lower temperatures when the doping increases. For the electron doped case the downturn is much flatter and moves very slowly to smaller temperatures with doping. The main effect of doping is to make the downturn flatter. We found an almost flat low-temperature spin susceptibility at 15% electron doping, which is an indication of Fermi-liquid behavior. A sharp downturn results in a rapid transition to the pseudogap physics, and we observed that at the same temperature the pseudogap in the hole doped case is more developed than in the electron doped case, even though the electron regime corresponding T^* is larger. Another interesting feature is the very strong increase of the uniform charge susceptibility for the electron-doped case in the underdoped region (5% doping), suggesting

a tendency for phase separation (see Chap. 7). With respect to the asymmetry of the d-wave pairing it can be noticed that above T_c the pairing correlations increases with the doping in the electron doped case and remains more or less the same (actually it slightly decreases) in the hole doped case. The superconductivity transition critical exponent is smaller in the hole doped case, indicating stronger fluctuations.

6.4 Reduction of Two-Band Hubbard Model to Single-Band Hubbard Model

An important conclusion of the previous section is that the electron-hole asymmetry is an intrinsic property of the CuO_2 plane. In this section we are going to address two closely related problems, one concerning the reason for the asymmetry and the other concerning the reduction of the two-band Hubbard model to a single-band Hubbard one.

In order to decide whether the low-energy physics of cuprate superconductors can be described by a single-band Hubbard Hamiltonian we are going to compare the one-particle spectral functions (density of states) and the two-particle properties (susceptibility functions) of the two-band and single-band Hubbard models. Without claiming that the similarity of the two models DOS and susceptibility functions would give a complete proof of the fact that the one-band Hubbard model is the effective Hamiltonian which describes the two-band Hubbard model low-energy physics *, we believe this is a compelling approach for establishing the validity of the Zhang and Rice assumption. The experimental information is obtained measuring the response functions behavior (and in almost all cases the two-particle operators or the one-particle ones, as in photoemission, are involved). It is also true that a comparison of the dynamic susceptibilities would be required, but with our Quantum Monte Carlo based algorithm the calculation of these quantities for the two-band model is extremely computational resources consuming and has not been done yet. However partial information about the relevant excited states is contained in the temperature behavior of the static susceptibilities.

If Zhang and Rice theory is right, the single-band Hubbard model suited for describing the physics of CuO_2 planes should include at least the next-nearest-neighbor hopping integral, therefore we start by comparing the two-band Hubbard model with a $t-t'-U$ single-band Hubbard model

$$H = -t \sum_{<i,j>,\sigma} d^{\dagger}_{i\sigma} d_{j\sigma} - t' \sum_{\ll i,j \gg,\sigma} d^{\dagger}_{i\sigma} d_{j\sigma} + U \sum_{i} n_{di\uparrow} n_{di\downarrow} \tag{6.29}$$

In Eq. 6.29 $< >$ and $\ll \gg$ means summation over the nearest-neighbor sites and respectively next-nearest-neighbor sites. The inclusion of higher than nearest-neighbor order hopping terms would be a necessary condition for explaining the electron-hole asymmetry, being known that a simple $t-U$ Hubbard model is symmetric with respect to electron and hole doping. Even if different parameters are used for the electron and respectively

*To prove this we should show that the matrix elements of the single-band Hubbard model resolvent operator are the same with the two-band Hubbard model ones corresponding to the low-energy states [28]. This would also imply a comparison of more-than-two-particle operators correlation functions.

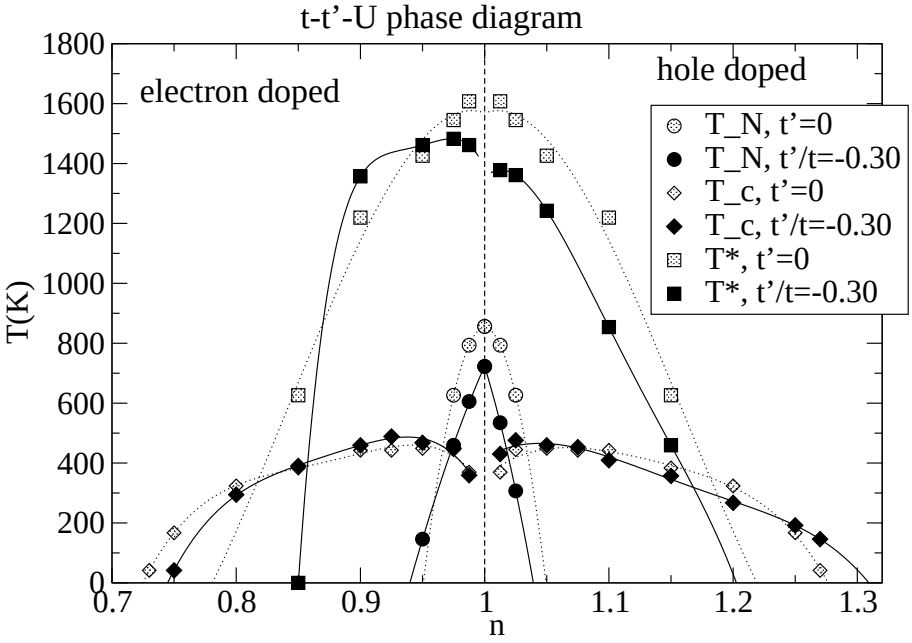

Figure 6.14: *t-t'-U Hubbard model (solid line) and t-U Hubbard model (dashed line) phase diagrams for* $t = -0.45\ eV,\ t'/t = -0.3, U = 0.3.6\ eV$.

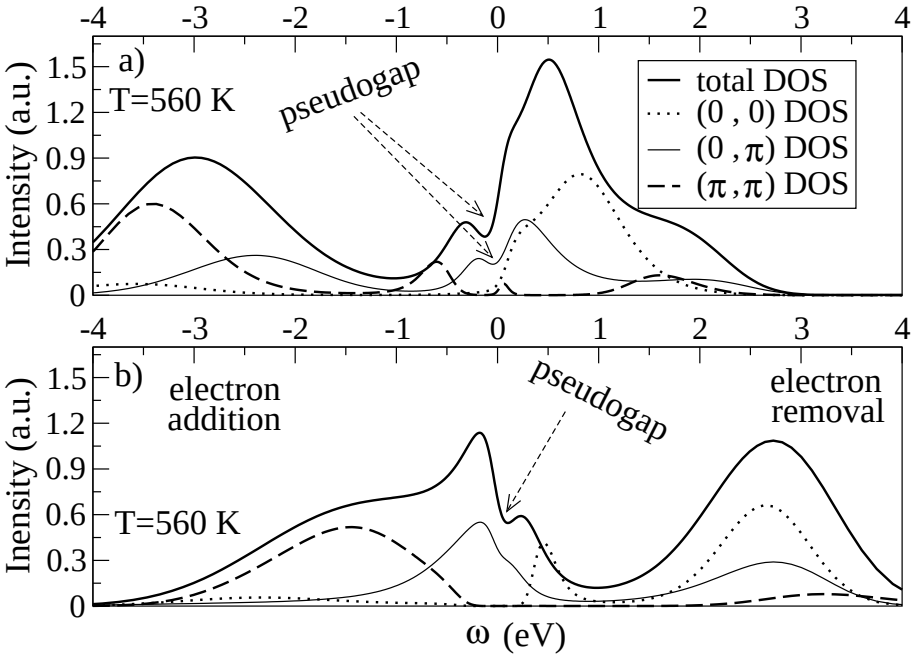

Figure 6.15: *a)* $t - t' - U$ *total DOS and coarse-grained* K *dependent DOS at* 5% *doping for* $t = -0.45\ eV,\ t'/t = -0.3, U = 0.3.6\ eV$. *a) hole doping case. b) electron doping case.*

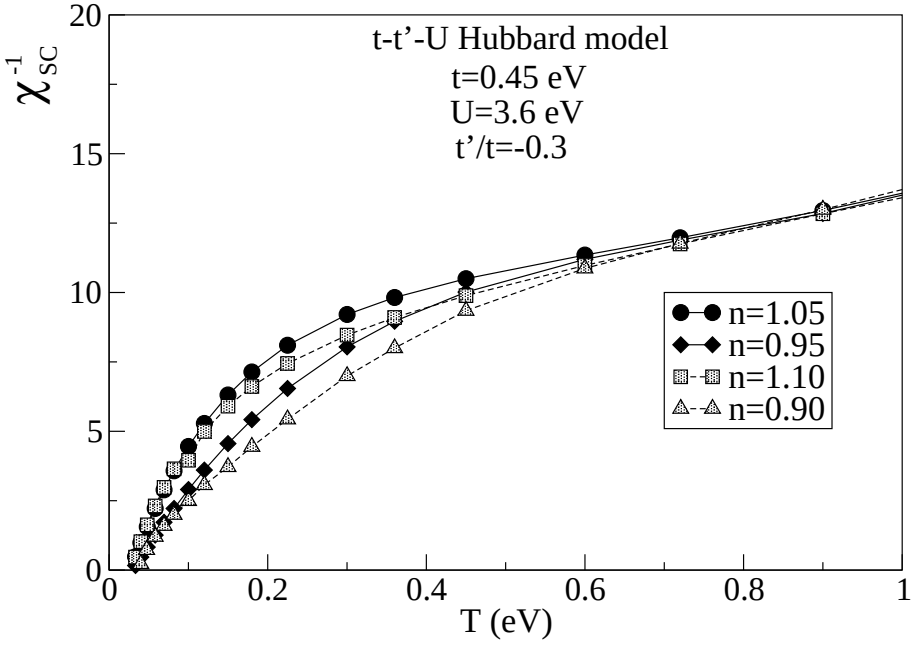

Figure 6.16: *t-t'-U Hubbard model. Inverse of the d-wave pairing susceptibility χ^{-1}_{SC} versus temperature for different hole densities.*

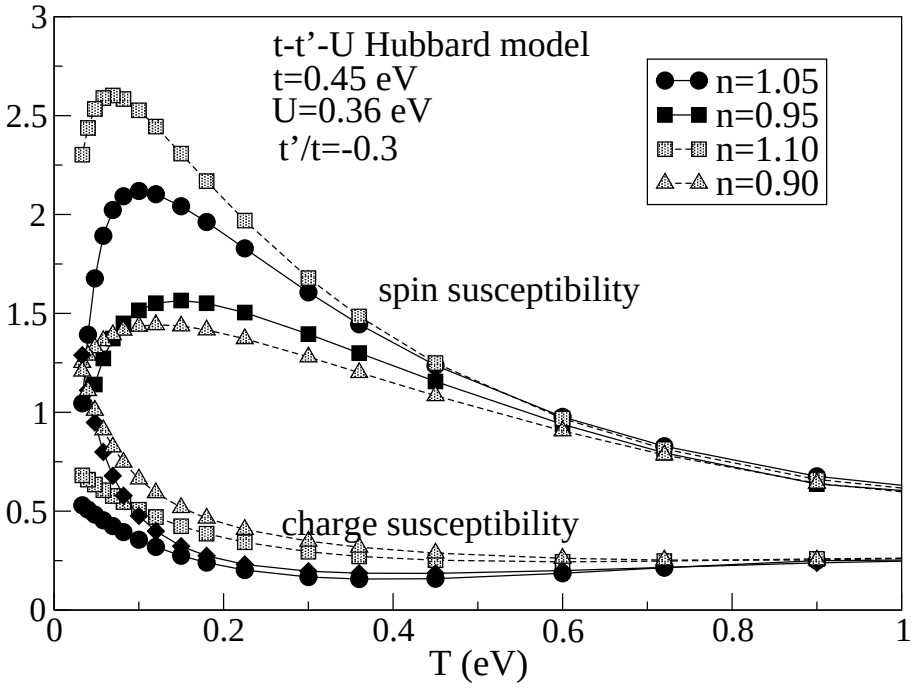

Figure 6.17: *t-t'-U Hubbard model. Uniform spin (upper part) and charge (lower part) susceptibilities versus temperature for different hole densities.*

for the hole doped regimes, some features like the susceptibilities behavior upon doping or the momentum dependent one-electron spectral functions could not be explained with a simple nearest-neighbor only hopping Hubbard Hamiltonian. The most significant higher order hopping parameter is the next-nearest-neighbor one, t', as explicitly cluster calculations show [29], which has different effective sign for the electron and respectively for the hole doped case. In a single-band $t-t'-U$ model the effective sign of t and t' is also different in the electron and in the hole representation. In the hole representation $t<0$ and $t'>0$. In order to avoid confusions we must specify that we define the hole (electron) representation as the one where the filling $1+\delta$ corresponds to the δ hole (electron) doping. The sign of t is only a matter of convention, the change of it would correspond to a translation with a (π,π) vector in the Brillouin Zone, but the t' hopping sign turns out to have a major influence on the Hubbard model physics.

We have found very similar physics for the two models. In Fig. 6.14 the phase diagram of the $t-t'-U$ model is shown with solid line *. In order to see the effect of t', the phase diagram of $t-U$ Hubbard model (i.e. $t'=0$ case) is also shown with dashed line. At half filling t' introduces an effective antiferromagnetic exchange $J'=4t'^2/U$ between the same sublattice spins and subsequently frustrates the antiferromagnetism. However at finite electron doping, t' favors the antiferromagnetism, making it persist up to a larger doping. On the other hand, in the hole doped case, the antiferromagnetism is always suppressed by t'. With respect to superconductivity, the presence of t' results in a smaller (larger) critical electron (hole) doping at which the superconductivity disappears. t' has no major influence on the maximum superconductivity critical temperature T_c^{max}.

In Fig 6.15 we present the $t-t'-U$ Hubbard model DOS at 5% doping. The one-particle spectral functions resemble the corresponding two-band Hubbard model ones. The presence of the t' parameter with the right sign is responsible for the location of the pseudogap in the Brillouin Zone (see also Fig. 7.7 where the DOS calculated for $N_c=8$ cluster is shown).

The d-wave paring susceptibilities shown in Fig. 6.16 exhibit similar asymmetric features as the corresponding two-band model ones. In the hole doped regime the t' hopping integral decreases the d-wave paring before the superconductivity transition and increases the pairing fluctuations (the critical exponent is smaller, the deviation from the mean field value 1 being larger).

The uniform spin and charge susceptibilities are shown in Fig. 6.17. The similarity to the two-band Hubbard model case is evident. The spin susceptibility at the pseudogap temperature T^* is strongly increasing with doping for the hole doped case and an opposite effect is seen for the electron doped case. The downturn at T^* in the spin susceptibility is much sharper for the hole doped regime indicating a fast transition to the pseudogap physics. The electron-doped charge susceptibility is strongly increased below T^* in the underdoped region, similar to what happens for the two-band Hubbard model.

The necessity of the t' hopping (and even of the third neighbor hopping t'') in explaining the measured ARPES line shape and the electron-hole asymmetry [30–36] was realized early on. Representing hopping terms on the same sublattice, these parameters are not severely renormalized in an antiferromagnetic background and therefore their influence

*Here we kept the sign of t' always positive and modified the density of holes, thus that the δ hole (electron) doping would correspond to $1+(-)\delta$ hole filling per unit cell.

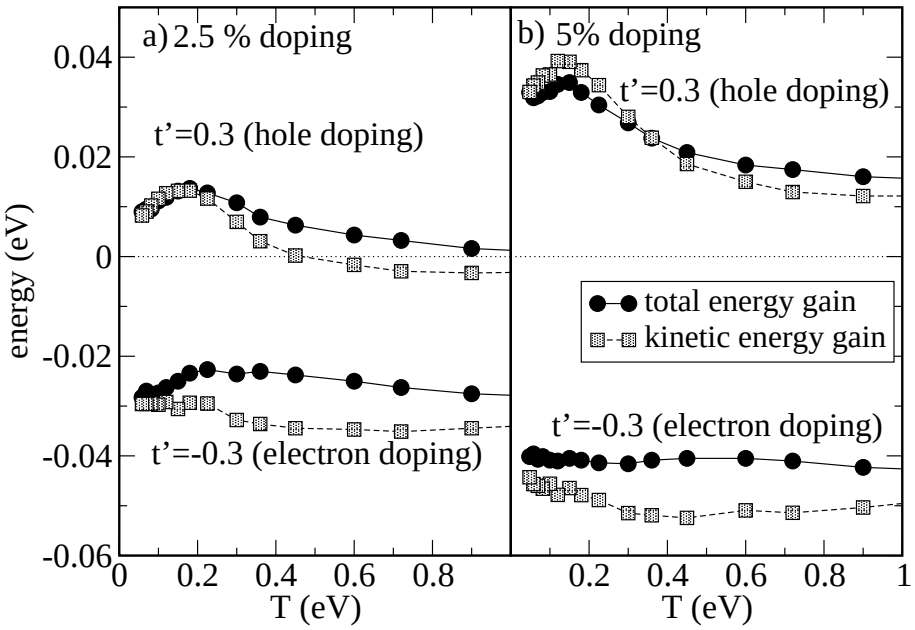

Figure 6.18: *The total energy gain (i.e.* $E_{total}(t' \neq 0) - E_{total}(t' = 0)$*) and the kinetic energy gain (i.e.* $E_{kinetic}(t' \neq 0) - E_{kinetic}(t' = 0)$*) when the* t' *parameter is switched on. The upper part corresponds to* $t' > 0$ *(i.e. hole doping) and the lower part to* $t' < 0$ *(i.e. electron doping). a) At* 1.025 *unit cell filling. b) At* 1.05 *unit cell filling.*

turns out to be important. The exact diagonalization results [34, 36] of the $t - t' - J$ model, which are in agreement with ours, are very helpful for understanding the t''s influence on the ARPES spectra and magnetic properties. The one hole in a $t - J$ model ($t' = 0$) calculation predicts a dispersion of the form

$$E_0(k) = -0.55J(\cos(k_x) + \cos(k_y))^2 \tag{6.30}$$

which is flat along the $(0, \pi) - (\pi, 0)$ direction, in disagreement with experiments. The introduction of t' would add the term

$$E_1(k) = -4t'_{eff} \cos(k_x) \cos(k_y) \tag{6.31}$$

with the t'_{eff} effective value roughly proportional with t', which will lift up the degeneracy. For positive t' (hole doped case) the lowest energetically addition state is at $(\pi/2, \pi/2)$ in the Brillouin Zone. For negative t' (electron doped case) the closest to the Fermi level particle addition states are situated at $(0, \pi)$ and $(\pi, 0)$. Exact diagonalization calculation shows that the hopping process with $t' < 0$ (electron doped case) is energetically favorable unlike the hopping with $t' > 0$ (hole doped case). The DCA results lead us to the same conclusion. In Fig. 6.18 the gain in the the total and in the kinetic energy when the t' hopping is switched on is shown at $\delta = +0.025$ and at $\delta = +0.05$ doping. For $t' < 0$ (electron doped) the system is lowering the total energy due to a large gain in the kinetic energy and a small loss in the potential energy. For $t' > 0$ (hole doped) the system has a larger energy due to the increase of kinetic energy. The Neel-type configurations are favorable to the next-nearest-neighbor hopping process, therefore for the electron

doped case these configurations are stabilized (which will result is a small increase in the potential energy and a large decrease in the kinetic energy) and the antiferromagnetism is enhanced. For the hole doped case the t' hopping process is discouraged and this leads to the suppression of antiferromagnetism.

We believe that the inclusion of t'' in a one-band Hubbard model will improve the agreement with the two-band model results. However for a quantitative comparison one has to be careful. The amplitude of the different one-band model parameters does not have necessarily to coincide in the electron and in the hole doped regimes, as cluster calculation shows explicitly [29]. The slightly doping dependent Cu-O covalency which we found for the two-band Hubbard model (Fig. 6.12-a) presumably implies modestly doping dependent parameters for the corresponding reduced one-band Hubbard model.

6.5 Conclusions

As a result of the large oxygen bandwidth in cuprates, as a starting point, any realistic model should take fully into account all the oxygen hopping integrals. Starting from a five-band Hubbard Hamiltonian which considers all the oxygen degrees of freedom which couple with the Cu $d_{x^2-y^2}$ orbitals we calculate the properties of the CuO_2 plane using the DCA technique on a 2×2 cluster.

We found that up to 40% hole doping only the oxygen band which couples directly with the Cu band is significantly occupied (the occupation of the other being less than 1%). This, together with a comparison of different properties of the five-band Hubbard Hamiltonian to the reduced two-band Hubbard Hamiltonian which shows very small difference between the two models, lead us to the following conclusions:

- The reduction of the five-band model to a two-band model which considers only the Cu $d_{x^2-y^2}$ and the oxygen $B1\sigma$ band is a good approximation for the low-energy physics of cuprates.

- The low-energy physics of the hole doped cuprates is determined by the mixed $d_{x^2-y^2} - B1\sigma$ states which are pushed out from the non-bonding oxygen bands as a consequence of the strong Cu-O hybridization. The non-bonding oxygen states do not contribute to the low-energy physics.

Calculating the two-band Hubbard model properties we found:

- The phase diagram resembles the generic phase diagram of the cuprates containing regions characterized by antiferromagnetism, pseudogap and d-wave superconductivity.

- The system is strongly covalent. In the electron doped regime the Cu-O mixing is slightly doping dependent, increasing with electron doping.

- The phase diagram, one-particle spectral functions and charge, spin and d-wave susceptibility functions show asymmetric features with respect to the electron and the hole doping regimes in agreement with experimental data, proving that this asymmetry is an intrinsic property of CuO_2 plane.

We compared the two-band Hubbard model properties with a single-band $t - t' - U$ Hubbard ones. If the Zhang and Rice theory is correct and the cuprates physics can be described by a one-band model, in order to explain the electron-hole asymmetric features at least the next-nearest-neighbor hopping term t' should be included. The t' has a different sign in the electron ($t' < 0$) and respectively in the hole ($t' > 0$) representation. We conclude the following:

- The two models exhibits very similar low-energy physics provided that the next-nearest-neighbor hopping term t' is set appropriately.
- The next-nearest-neighbor hopping term t''s sign is the principal culprit for the observed electron-hole asymmetry.
- The mapping of the two-band Hubbard model into a single-band one is a good approximation, as Zhang and Rice theory claims, provided we include the t' hopping.

References

[1] J. Zaanen, G. A. Sawatzky, and J. W. Allen, Phys. Rev. Lett. **55**, 418 (1985).

[2] D. Jorgensen, H. B. Schuttler, D. G. Hinks, D. W. Capone, K. Zhang, M. B. Brodsky, and D. J. Scalapino, Phys. Rev. Lett. **58**, 1024 (1987).

[3] L. F. Mattheis, Phys. Rev. Lett. **58**, 1028 (1987).

[4] J. Yu, A. J. Freeman, and J. H. Xu, Phys. Rev. Lett. **58**, 1035 (1987).

[5] C. M. Varma and S. Schmitt-Rink, Solid State Com. **62**, 681 (1987).

[6] V. J. Emery, Phys. Rev. Lett. **58**, 2794 (1987).

[7] V. J. Emery and G. Reiter, Phys. Rev. B **38**, 4547 (1988).

[8] F.C.Zhang and T.M.Rice, Phys. Rev. B **37**, 3759 (1988).

[9] H. Eskes, L. J. Tjeng, and G. A. Sawatzky, Phys. Rev. B **41**, 288 (1990).

[10] E. B. Stechel and D. R. Jennison, Phys. Rev. B **38**, 4632 (1988).

[11] M. S. Hybersten, M. Scluter, and N. E. Christen, Phys. Rev. B **39**, 9028 (1989).

[12] H. Eskes and G.A.Sawatzky, Phys. Rev. Lett. **61**, 1415 (1988).

[13] V.J.Emery and G.Reiter, Phys. Rev. B **38**, 11938 (1988).

[14] F.C.Zhang and T.M.Rice, Phys. Rev. B **41**, 7243 (1988).

[15] V.J.Emery and G.Reiter, Phys. Rev. B **41**, 7247 (1990).

[16] C. Almasan and M. B. Maple, in *Chemistry of High-Temperature Superconductors*, edited by C. M. R. Rao (World Scientific, Singapore, 1991).

[17] E.Dagotto, Rev. Mod. Phys. **66**, 763 (1994).

[18] N. P. Armitage, *et al.*, Phys. Rev. Lett. **88**, 257001 (2002).

[19] B. O. Wells, *et al.*, Phys. Rev. Lett. **74**, 964 (1995).

[20] A. K. Mcahan, J. F. Annett, and R. M. Martin, Phys. Rev. B **42**, 6268 (1990).

[21] M. Jarrell and J. E. Gubernatis, Phys. Rep. **269**, 135 (1996).

[22] S. Moukouri and M.Jarrel, Phys. Rev. Lett. **87**, 167010 (2001).

[23] W. W. Warren, *et al.*, Phys. Rev. Lett. **62**, 1193 (1989).

[24] M. Takigawa, *et al.*, Phys. Rev. B **43**, 247 (1991).

[25] H. Alloul, *et al.*, Phys. Rev. Lett. **70**, 1171 (1993).

[26] M. Takigawa, *et al.*, Physica C **162-164**, 853 (1989).

[27] M. Takigawa, in *High-Temperature Superconductivity*, edited by K. Bedell, D. Coffey, D. E. Meltzer, D. Pines, and J. R. Schrieffer (Addison-Wesley, 1990), p. 236.

[28] A. Auerbach, *Strongly Interacting Electrons and Quantum Magnetism* (New York, Springer-Verlag, 1994).

[29] H. Eskes, G. A. Sawatzky, and L. Feiner, Physica C **160**, 424 (1989).

[30] A. Nazarenko, K. J. Vos, S. Haas, E. Dagotto, and R. Gooding, Phys. Rev. B **51**, 8676 (1995).

[31] P. W. Leung, B. O. Wells, and R. J. Gooding, Phys. Rev. B **56**, 6320 (1997).

[32] R. Eder, Y. Ohta, and G. A. Sawatzky, Phys. Rev. B **55**, R3414 (1997).

[33] O. P. Sushkov, G. A. Sawatzky, R. Eder, and H. Eskes, Phys. Rev. B **56**, 11769 (1997).

[34] T. Tohyama and S. Maekawa, Supercond. Sci. Technol. **13**, R17 (2000).

[35] T. Tohyama and S. Maekawa, Phys. Rev. B **49**, 3596 (1994).

[36] T. Tohyama and S. Maekawa, Phys. Rev. B **64**, 212505 (2001).